2007 IEEE International Conference on
Robotics and Automation
Roma, Italy, 10-14 April 2007

Real-Time High-Accuracy Micropipette Aspiration for Characterizing Mechanical Properties of Biological Cells

Xinyu Liu, *Student Member, IEEE*, Yifei Wang, Yu Sun, *Member, IEEE*

***Abstract* –This paper presents a micropipette aspiration system and a cell contour visual tracking algorithm for real-time, high-accuracy mechanical characterization of individual cells. The computer vision tracking algorithm measures cell deformation parameters in real time (30Hz) with a resolution down to 0.21 pixel, significantly enhancing the accuracy and efficiency of the micropipette aspiration technique. Representing another advantage over manual measurements in terms of characterization accuracies, the micropipette aspiration system features precise synchronization between cell deformations and applied pressure changes. Experimental results on both solid-like cells (interstitial cells) and liquid-like cells (neutrophils) demonstrate the effectiveness of the system and the visual tracking algorithm. Among several characterized mechanical parameters, the viscoelastic properties of porcine aortic valve interstitial cells were, for the first time, quantified in this study.**

I. Introduction

MECHANICAL signals (i.e., applied forces and stresses) are capable of regulating the phenotypic expression of biological cells. These mechanical stimuli are particularly important for highly mechanically responsive cells such as cardiovascular, musculoskeletal, and bone cells. For example, it has been demonstrated that mechanical forces play a major role in the regulation of cell adhesion and cytoskeletal organization [1]. While it is important to investigate how mechanical forces/stresses regulate cell responses, it is also significant to characterize the mechanical properties of individual cells for understanding cellular structures and predicting their response to mechanical stimuli.

For measuring mechanical properties of a living cell, the cell must be deformed in some way by a known force or stress and its deformations measured. Besides atomic force microscopy [2], laser trapping [3], magnetic bead measurements [4], and microelectromechanical systems (MEMS) based force measurements [5], micropipette aspiration is a very popular technique for quantifying mechanical properties of individual cells, such as modulus and viscosity [6].

As shown in Fig. 1, the micropipette aspiration technique applies a sucking pressure ΔP to deform a cell, and a portion of the cell is elongated into the micropipette. Continuum models are used to treat the cell either as a homogeneous elastic solid [7][8] or as a liquid surrounded by an elastic cortical shell [9][10]. Experimentally, solid cells and liquid cells are different in response to a critical pressure [6]. For liquid-like cells (e.g., neutrophils [9][10] and erythrocytes [11]), an applied pressure above the critical value causes complete cell aspiration into the micropipette. On the other hand, a cell exhibiting behavioral characteristics of a solid (e.g., endothelial cells [7][8] and chondrocytes [12]) continues to enter a finite distance into the micropipette when applied pressure exceeds the critical value. For characterizing both solid-like and liquid-like cells, the applied negative pressure ΔP and the resulting aspiration length (L) must be experimentally measured. Additionally, characterizing liquid-like cells also requires the radius of the cell contour outside the micropipette (R_c) to be measured.

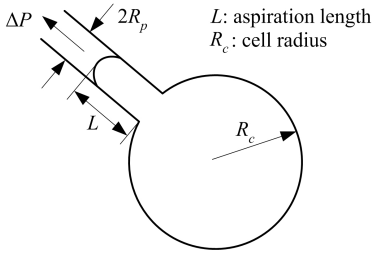

Fig. 1 Schematic of micropipette aspiration.

Key experimental factors that determine the validity of mechanical characterization results include the accuracy of applied pressure, the accuracy of cell geometrical parameter measurements, and the synchronization of applied pressure and resulting geometrical changes of the cell. Currently, cell deformation images and pressure data are acquired separately, and synchronization is roughly estimated. A large number of images (30 frames/sec for minutes) are recorded by a VCR for post processing in which cell contours are manually measured with a cursor on the video screen. Cell contour measurements are tedious for human operators, making micropipette aspiration a time consuming technique. More importantly, off-line manual measurements produce significant errors in subsequent mechanics modeling due to the low accuracy of manual measurements and the poor synchronization of cell contour images and pressure data. In the most ideal case, manual measurements are still limited to a resolution of one image pixel. Thus, the development of a high-accuracy micropipette aspiration system, integrating a precise synchronization mechanism and a computer vision tracking algorithm capable of conducting cell contour measurements in real time (30 frames/sec) with a sub-pixel resolution, is highly desired.

This paper presents a sub-pixel cell contour visual tracking algorithm, a micropipette aspiration system with a precise synchronization mechanism, and their application to conducting real-time, high-accuracy micropipette aspiration. The images of deformed cell contours and sucking pressure data are precisely synchronized on a host computer. The visual tracking algorithm is capable of measuring the parameters of cell contour in real time during the aspiration

The authors are with the Advanced Micro and Nanosystems Laboratory at the University of Toronto. 5 King's College Road, Toronto, Canada, M5S 3G8 (phone: 1-416-946-0549; e-mail: sun@mie.utoronto.ca).

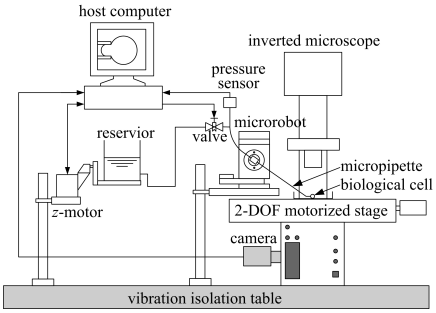

Fig. 2 Schematic diagram of the micropipette aspiration system.

process, enabling online characterization of cellular mechanical properties. Experiments demonstrate that this computer vision-based system greatly improves the accuracy and efficiency in cellular mechanical property characterization using the micropipette aspiration technique.

II. Micropipette Aspiration System Setup

The experimental system, schematically shown in Fig. 2, consists of an inverted microscope (Olympus IX81) with a CMOS camera (Basler A601f), a 3-DOF microrobot (Sutter MP-285) for positioning the micropipette, a 2-DOF motorized stage (Prior Scientific ProScan II) for positioning samples, a sucking pressure system for generating well controlled negative pressures, and a host computer with a data acquisition card (NI PCI-6229) for cell contour visual tracking and pressure data acquisition. The sucking pressure system includes an adjustable water reservoir, a *z*-motor, a solenoid valve, and a pressure sensor (AllSensors U.S.). Pressure is controlled by adjusting the height of the reservoir using the *z*-motor. The pressure sensor is located close to the micropipette tip to minimize the pressure-transmission-caused time lag between pressure measurements and applied pressure. The measurement resolution of the pressure sensor is 0.1Pa. The system setup is mounted on a vibration isolation table for minimizing vibration. In contrast to existing micropipette aspiration systems [8][12] that use VCR image recording and multiplexing display of pressure data, the microscopic images and sucking pressure data in our system are directly acquired and processed by the host computer, enabling precise synchronization of cell deformations and sucking pressure. The lapse time between the acquisitions of the two types of signals is less than 5ms.

III. Continuum Models

Two types of micropipette aspiration continuum models are typically used for characterizing the mechanical properties of solid-like and liquid-like cells. For solid-like cells, the homogenous half-space models [7][8] are used for quantifying elastic and viscoelastic parameters. For liquid-like cells, the cortical shell-liquid core models [9][10] are employed. In order to facilitate the discussion in Section V, these continuum models are briefly described as follows.

A) Homogeneous Half-Space Models

This model considers the entire cell as a homogeneous solid body. With linear elasticity assumed, the relationship between aspiration length into the micropipette (L) and the sucking pressure is [7]

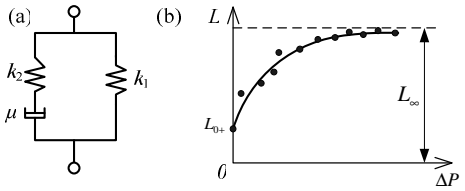

Fig. 3 Homogeneous viscoelastic half-space model. (a) The Kelvin model. (b) A typical cell response curve to stepwise sucking pressures.

$$\Delta P = \frac{2\pi}{3\phi} E \frac{L}{R_p} \tag{1}$$

where E is the Young's modulus of the homogeneous solid, ΔP is the sucking pressure, R_p is the inner diameter of the micropipette, and ϕ is a wall function determined by the pipette dimension and has a typical value of 2.1. The measurement accuracy of ΔP and L determines the accuracy of the Young's modulus E.

In order to account for the viscoelastic response of biological cells, the Kelvin model (Fig. 3(a)), a standard linear viscoelasticity model, is commonly used for establishing a homogeneous half-space viscoelastic model. When a stepwise sucking pressure is applied to the cell, cell deformations are [8]

$$L(t) = L_\infty \left[1 - \frac{k_2}{k_1 + k_2} \exp\left(-\frac{t}{\tau} \right) \right] h(t) \tag{2}$$

where

$$L_\infty = \lim_{t \to \infty} L(t) = \frac{2 R_p \Delta P}{\pi k_1} \tag{3}$$

$h(t)$ is a unit step function,

$$h(t) = \begin{cases} 1 & t > 0 \\ 0 & t < 0 \end{cases} \tag{4}$$

k_1 and k_2 are the elastic constants in the Kelvin model, and τ is a time constant given by

$$\tau = \frac{\mu}{k_1} \left(1 + \frac{k_1}{k_2} \right) \tag{5}$$

where μ is the coefficient of viscosity in the Kelvin model.

The typical cell response curve is shown in Fig. 3(b). The aspiration length asymptotically reaches equilibrium. From (2), the initial aspiration length (L_{0+}) due to the elastic effect can be derived as

$$L_{0+} = \frac{k_1}{k_1 + k_2} L_\infty \tag{6}$$

k_1 is experimentally obtained by measuring the asymptotic length of the elongated portion L_∞. k_2 is experimentally obtained by measuring L_∞ and L_{0+}. Fitting (2) to the experimental data determines τ and μ. In existing micropipette aspiration systems, the measurement of L_{0+} is extremely difficult due to poor synchronization in [8], which introduces significant errors into k_2.

B) Cortical Shell-Liquid Core Models

A critical pressure is defined in the deformation response of liquid-like cells as the pressure causing a hemispherical

cellular projection into the micropipette [6]. When the sucking pressure is below the critical value, aspiration length is almost linear; however, a sucking pressure above the critical value causes the cell to automatically flow into the micropipette. An application of the Laplace law to the aspiration of liquid-like cells results in the following equilibrium equation [9][10]

$$\Delta P = 2T_c\left(\frac{1}{R_p}-\frac{1}{R_c}\right), \quad \left(\Delta P = \Delta P_c \text{ when } \frac{L_p}{R_p}=1\right) \tag{7}$$

where T_c is the cortical tension, R_c is the radius of the cell portion outside the pipette, and ΔP_c is the critical pressure. The accurate measurement of ΔP_c also requires precise synchronization of cell deformations and pressure data.

The viscoelastic properties of liquid-like cells can be characterized by measuring the rate at which a cell flows into the micropipette in response to a stepwise sucking pressure. Cytoplasm viscosity is estimated by [10]

$$\eta = \frac{R_p \Delta P}{\left(\frac{dL}{dt}\right)m\left(1-\frac{R_p}{R_{cm}}\right)} \tag{8}$$

where m is a constant with a typical value of 6, and R_{cm} is the radius of the outer cell portion corresponding to the middle point in the linear region of L vs. time in experimental data.

IV. Cell Contour Visual Tracking

In order to accurately measure cell deformation parameters (L and R_c in Fig. 1), a sub-pixel visual tracking algorithm is developed. For the measurement of aspiration lengths (L), the micropipette tip and the *leading* edge of the aspirated cell portion must be precisely located. For the measurement of cell outer radius (R_c), the cell contour outside the micropipette is accurately tracked. In this study, an identification algorithm is developed to locate the micropipette tip, providing a reference position for the measurement of L. A canny edge detector with adaptive thresholding is employed to detect the cell contour outside the micropipette. A Kalman tracking algorithm is responsible for tracking the leading edge that projects into the micropipette. The current implementation assumes that the cell locates to the right of the micropipette; however, the algorithm can be readily modified to account for location differences.

In the following description, all images are first smoothed by a low-pass Gaussian filter, and the resulting images are denoted by $I_i(x, y)$.

A) Micropipette Tip Identification

In order to measure the length of cell projection into the micropipette, an identification algorithm is developed to locate the micropipette tip in the first frame of image where the establishment of initial contact between the cell and the side wall of the micropipette tip occurs. This contact blurs the vertical edge of the side wall. The edge of the cell in the proximity of the micropipette tip makes it difficult to precisely locate the micropipette tip using conventional edge detection algorithms, such as the Canny edge detector.

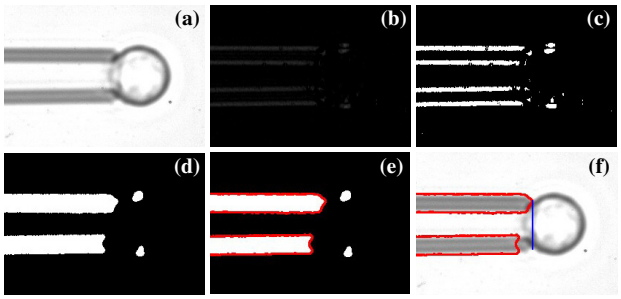

Fig. 4 Image sequence of micropipette tip identification. (a) Smoothed image of the first frame. (b) After gradient subtraction. (c) Adaptively thresholded. (d) Dilated image. (e) Top and bottom edges of micropipette walls found in (d). (f) Identified tip location.

1) Gradient subtraction: In our study, most of the edge information from the cell in the very first image frame is first removed using a gradient subtraction method. The absolute horizontal gradient is subtracted from the absolute vertical gradient in the first image frame. The resulting image (Fig. 4(b)) is

$$D_1(x, y) = \left|\nabla_y I_1(x, y)\right| - \left|\nabla_x I_1(x, y)\right| \tag{9}$$

2) Adaptive thresholding: $D_1(x, y)$ is adaptively thresholded and converted into a binary image $B_1(x, y)$ (Fig. 4(c)) using the Otsu method [13].

3) Morphological operation: A morphological close operation is used to connect the outer edge and inner edge of each micropipette wall into a single contour (Fig. 4 (d)).

4) Tip identification: By finding the two contours that span the greatest horizontal distance in the binary image $B_1(x, y)$, the top and bottom edges of the micropipette walls are found (Fig. 4(e)). The horizontal image coordinate of the rightmost point in these two contours is identified as the location of the micropipette tip (Fig. 4(f)).

The identified micropipette tip is then used as a reference position for tracking cell deformations, L and R_c. The processing time for tip identification is approximately 100ms. In experiments, the location of the micropipette tip is kept unchanged during the subsequent cell aspiration process. Thus, the micropipette tip identification is conducted only once, and does not sacrifice the real-time cell tracking.

B. Tracking of Cell Contour Outside Micropipette

1) Canny edge detector with adaptive thresholding: The Canny edge detector tracks local maxima of an image gradient and eliminates weak edges by hysteresis thresholding using two constant threshold values. The high threshold, T_h, is used to detect strong edges while the low threshold, T_l, detects weaker edges that are connected to strong edges. Due to the fact that different cell types reveal different image features, instead of frequently adjusting these two constant threshold values to accommodate different cell types, an adaptive thresholding algorithm for Canny edge detection [14] is employed in our study for tracking the cell contour outside the micropipette.

In the adaptive thresholding method, the histogram $H(i)$ from the gradient magnitude of the image $D_1(x, y)$ is first calculated, and the maximum value $H_{\max}$ is determined. The deviation of $H(i)$ from $H_{\max}$ is given by

$$\sigma = \sqrt{\sum_{i=0}^{N} [H(i) - H_{\max}]^2 / N} \qquad (10)$$

Accordingly, T_h is set to be $H_{\max}+\sigma$. The deviation σ' of $H(i)$ from $H_{\max}$ is re-calculated to exclude those pixels with gradient magnitudes above T_h. Finally, the low threshold value is determined as $T_l = H_{\max} + \sigma'$. Fig. 5(b) shows the result after Canny edge detection with adaptively determined threshold values and a morphological close operation that is used to connect the Canny detected edges of the cell contour and micropipette walls into a single contour (shown in red).

2) Radius measurement: After edge detection and close operation, the cell contour outside the micropipette (Fig. 5(c)) is extracted from the edge of the cell contour and micropipette walls (Fig. 5(b)) using the location information of the micropipette tip. In order to accurately determine the radius of the cell portion outside the micropipette R_c, a least square circle fitting algorithm [15] is used to fit the extracted cell contour into a circle for continuous measurements.

C. Tracking of Aspiration Lengths Into Micropipette

Once the micropipette tip and the cell center are identified in the first frame of image, two separate regions of interest (ROI), shown in Fig. 5(d), are determined and set for the subsequent tracking process. One ROI, to the right of the micropipette tip, is set to contain the cell portion outside the micropipette. The other ROI is to the left of the micropipette tip and contains the interior of the micropipette. The two ROIs are both symmetrical along the horizontal axis crossing the detected cell center.

The leading edge projecting into the micropipette must be accurately tracked in order to obtain accurate measurements of aspiration lengths L. However, the aspirated portion usually does not have a very distinct border, appearing rather faint. Active contour algorithms, such as *Snakes*, were found not to be capable of providing robust tracking performance due to the difficulty of controlling the snake's potential field to locate the leading edge. Snakes are particularly susceptible to the noise in the micropipette and the intracellular features that are often more prominent than the leading edge.

A Kalman tracking algorithm is developed that is capable of detecting weak edges and is robust to noises. The algorithm first obtains a horizontal gradient magnitude from the ROI that contains the leading edge. A low threshold is applied to the gradient for detecting the weak leading edge and producing a binary image. For example, a value of 20 was effective for human neutrophils in our experiments. All contours in the binary image are detected into chain code, and the area for each contour is calculated. The leading edge is determined by selecting the leftmost contour with an area above a threshold value that is set proportional to the inner diameter of the micropipette, by which most of the noisy contours are excluded. The horizontal coordinate of the leftmost point in the leading edge is regarded as the preliminarily measured position. To further improve tracking robustness, this measured position is processed by a Kalman filter [16] to predict the real location of the leading edge and eliminate disturbances from the noisy points.

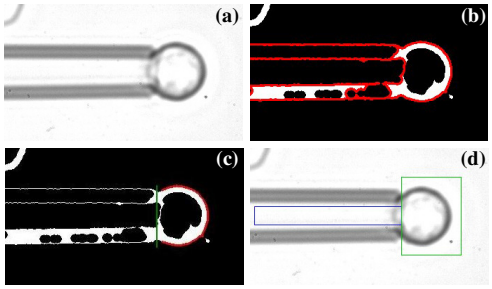

Fig. 5 Image sequence of tracking cell contour outside micropipette. (a) Smoothed image. (b) After adaptively thresholded Canny edge detection. (c) Cell contour determination using tip location information. (d) Determination of ROIs for subsequent tracking.

Briefly, the Kalman filter uses a state vector $\mathbf{X}_i = [x_i, x_{i-1}, x_{i-2}]^T$ that consists of the estimated real positions of the leading edge in the past three images. A transition matrix is used to model the dynamics of the edge with the assumption of constant acceleration.

$$\mathbf{A} = \begin{bmatrix} 3 & -3 & 1 \\ 1 & 0 & 0 \\ 0 & 1 & 0 \end{bmatrix}$$

The prediction step of the Kalman cycle is given by

$$\mathbf{X}'_i = \mathbf{A}\mathbf{X}_{i-1} \qquad (11)$$

where $\mathbf{X}'_i$ is the predicted state vector. Updating is conducted according to

$$\mathbf{X}_i = \mathbf{X}'_i + \mathbf{K}_i(z_i - \mathbf{H}\mathbf{X}'_i) \qquad (12)$$

where $\mathbf{K}_i$ is the Kalman gain [16], z_i is the measured position of the leading edge, and $\mathbf{H}$ = [1 0 0]. The real position of the leading edge is finally determined by

$$z'_i = \mathbf{H}\mathbf{X}_i \qquad (13)$$

V. Experimental Results

The micropipette aspiration system and the sub-pixel cell contour visual tracking algorithm were applied to characterizing mechanical properties of solid-like porcine aortic valve interstitial cells (PAVIC) and liquid-like human neutrophils. Both elastic and viscoelastic properties of these two types of cells were quantified.

A 60× objective (NA 0.7) plus a 1.6× coupler, and bright-field imaging were used for observing the cells. The calibrated pixel size is 0.11μm×0.11μm. Images and pressure data were acquired at the frequency of 30Hz. The cell contour visual tracking algorithm cost 10.2ms for processing each frame of image, proving the real-time capability for measuring cell parameters. For PAVICs, the tracking resolution of L is 0.21 pixel. For human neutrophils, the tracking resolution is 0.29 pixel for L and 0.42 pixel for R_c.

A) Characterization of PAVICs

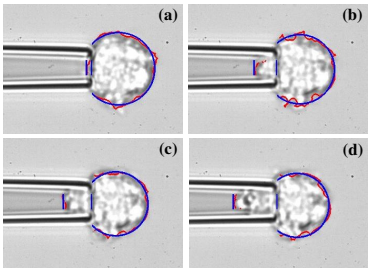

Fig. 6 Micropipette aspiration of a porcine aortic valve interstitial cell.

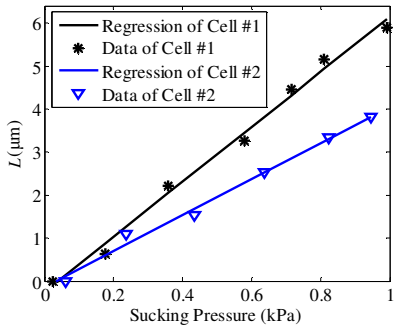

Fig. 7 PAVIC deformation data L vs. sucking pressure.

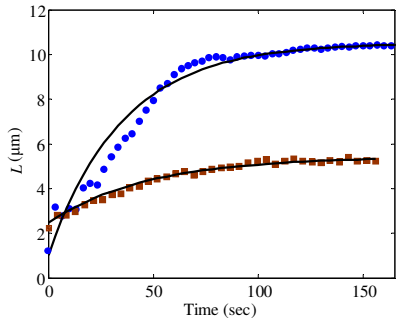

Fig. 8 Viscoelastic response of PAVICs.

TABLE I PAVIC VISCOELASTIC PARAMETERS (BASED ON FIVE CELLS)

Parameters	k_1 (Pa)	k_2 (Pa)	τ (s)	μ (Pa·s)
Values	154±60	311±70	45±12	4330±958

1) PAVIC preparation: Aortic valve leaflets were harvested from healthy pig hearts, and interstitial cells were enzymatically isolated. The cells were grown on tissue culture flasks and were kept in an incubator in standard tissue culture medium (DMEM supplemented with 10% FBS and 1% antibiotics). The medium was changed every 2 days, and the cells were passaged when confluent. P2 cells were trypsinized and re-suspended in standard tissue culture medium at 10^5 cells/mL for use in the experiments. A total of ten PAVICs were tested.

2) Measurements of Young's modulus: The average diameter of the PAVICs used in the experiments is 14.2μm, and the average inner diameter of the micropipette is 4.6μm. An initial tare pressure (~40Pa for 60sec) was applied to the cell to form a seal between the micropipette and the cell (Fig 6(a)). Sucking pressure in 6-8 increasing steps from 0.04kPa to 1kPa was then applied to deform the cell. An interval of 60sec between two adjacent steps allowed the cell to reach equilibrium. Fig. 6 shows the procedure of aspirating a PAVIC and the tracking results.

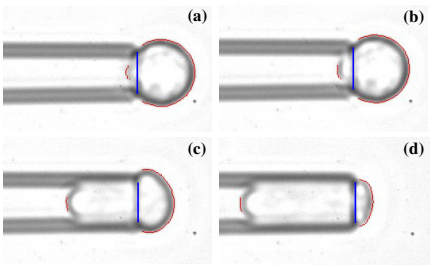

Fig. 9 Micropipette aspiration of a human neutrophil. (a) Initial state after the establishment of a seal. (b) The critical state. (c) Deformed cell flowing half-way into micropipette. (d) Cell completely flowing into micropipette except the hemispherical portion.

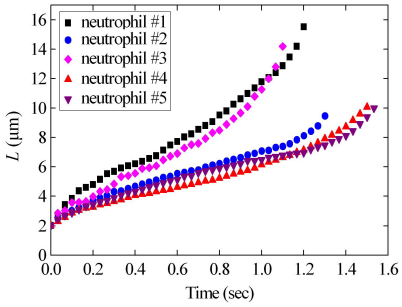

Fig. 10 Neutrophil tracking results of aspiration lengths into micropipette.

The aspiration lengths (L) were on-line measured by the sub-pixel cell contour tracking algorithm. Two representative sets of tracking data (L) vs. sucking pressure are shown in Fig. 7. The Young's modulus values of 345.8±142.5Pa were obtained according to (1), based on the measurements of five PAVICs. This result is comparable to the previously reported data of PAVICs (~449Pa) [17].

3) Measurements of viscoelastic properties: To date, there are no reported results on the viscoelastic properties of PAVICs. In this study, the viscoelastic properties of the PAVICs were quantified using the Kelvin model. A sucking pressure step of 860Pa (standard deviation ±56.7Pa) was applied to the PAVICs while resulting aspiration lengths L were measured in real time. The initial elastic response L_{0+}, was precisely measured, and a high accuracy is warranted by the precise synchronization in our system. The experimental data were fitted to exponential response curves using (2), and the parameters of k_1, k_2, τ, and μ in the model were computed according to (3), (5), and (6). Fig. 8 shows two representative sets of tracking results of L and the fitted curves. The statistics of the five aspirated PAVICs are summarized in Table I.

Compared with the reported characterization results of porcine aortic endothelial cells [8], which are another type of solid-like cells, the elastic constants of the PAVICs, k_1 and k_2, are approximately twice those of the endothelial cells, and the viscosity coefficient of the PAVICs, μ, is about half of the value of the endothelial cells. These results indicate that the PAVICs have a higher stiffness and a lower viscosity than porcine aortic endothelial cells.

B) Characterization of Liquid-Like Cells

1) Human neutrophil preparation: Neutrophils used in the experiments were isolated from 5ml of blood from a

healthy volunteer using one-step Polymorphprep (Accurate Chemical, Westbury, NY) and were suspended in Hanks' balanced salt solution (HBSS) with 10% compatible plasma.

2) Measurements of cortical tension and viscosity: Fig. 9 shows the procedure of aspirating a neutrophil and the tracking results. The inner diameter of the micropipettes used in the experiments is 4um. The average diameter of the neutrophils is 8.4μm. In the beginning of aspiration, the sucking pressure was controlled to increase until the aspiration length was equal to the micropipette radius, which was measured on line by the cell contour tracking algorithm. The critical pressure and the radius R_c at this point were automatically recorded by the system to calculate the cortical tension according to (7). After this critical point, the sucking pressure was increased by a step to 820Pa (standard deviation ±48.8Pa), causing the cell to automatically flow into the micropipette. During this process, the aspiration lengths and the radius of the cell portion outside the micropipette were measured in real time. Finally, the measured parameters were used to quantify the cell viscosities.

Fig. 10 shows the tracking results of aspiration lengths L for five tested neutrophils. The linear regions of these curves were fitted to calculate the constant flowing velocities. The measured flowing velocities and the stepwise sucking pressure (100±12.2Pa) were finally substituted into (8) for determining viscosities. For the five tested neutrophils, viscosity is 191.9±86.1Pa·s, and the determined cortical tension is 40.9±10.8pN/μm, which are comparable with previously reported results [9][10] (~135Pa·s for viscosity and ~35pN/μm for cortical tension).

VI. Discussion

The micropipette aspiration system and the cell contour tracking algorithm experimentally demonstrated high accuracy and high efficiency: cell deformation parameters were measured in real time (10.2ms for processing each frame of image) with a resolution down to 0.21 pixel. Another improvement over manual measurements is the precise synchronization of cell deformations and pressure changes, which is important for enhancing the measurement accuracy of the initial elastic response L_{0+} for solid-like cells in viscoleasticity characterization. Thus, a high accuracy of the elastic constant k_2 in the Kelvin model is attained. The precise synchronization mechanism also warrants a high measurement accuracy of the critical pressure for characterizing liquid-like cells.

VI. Conclusion

This paper reported on a micropipette aspiration system that features real-time, sub-pixel cell contour visual tracking with a resolution down to 0.21 pixel and precise synchronization between cell deformations and applied pressure. The visual tracking algorithm and the micropipette aspiration system provide a higher accuracy and efficiency than manual measurements, representing advancements in the micropipette aspiration technique. The cell contour tracking algorithm and the experimental system were applied to conduct micropipette aspiration experiments on porcine aortic valve interstitial cells and human neutrophils. The elastic and viscoelastic parameters of these cells were quantitatively obtained.

Acknowledgements

This research was supported by the Natural Sciences and Engineering Research Council of Canada. The authors thank Chris Moraes, Edmond Young, and Prof. Craig Simmons for assistance with interstitial cell preparations, and Profs. Gregory Downey and Michael Glogauer for the assistance with human neutrophils preparations.

References

[1] C.S., Chen, M. Mrksich, S. Huang, G.M. Whitesides, and D.E. Ingber, "Geometric control of cell life and death," *Science*, Vol. 276, pp. 1425-1428, 1997.

[2] E.K. Dimitriadis, F. Horkay, J. Maresca, B. Kachar and R.S. Chadwick, "Determination of elastic moduli of thin layers of soft material using the atomic force microscope," *Biophys. J.*, Vol. 82, pp. 2798-2810, 2002.

[3] J.W. Dai and M.P. Sheetz, "Mechanical properties of neuronal growth cone membranes studied by tether formation with laser optimal tweezers," *Biophys. J.*, Vol. 68, pp. 988-996, 1995.

[4] A.R. Bausch, F. Ziemann, A.A. Boulbitch, K. Jacobson, and E. Sachmann, "Local measurements of viscoelastic parameters of adherent cell surfaces by magnetic bead microrheometry, " *Biophys. J.*, Vol. 75, pp. 2038-2049, 1998.

[5] Y. Sun, K.T. Wan, B.J. Nelson, J. Bischof, and K. Roberts, "Mechanical property characterization of the mouse zona pellucida," *IEEE Trans. on NanoBioSci.*, Vol. 2, No. 4, pp. 279-286, 2003.

[6] R.M. Hochmuth, "Micropipette aspiration of living cells," *J. of Biomech.*, Vol. 33, pp. 15-22, 2000.

[7] D.P. Theret, M.J. Levesque, M. Sato, R.M. Nerem, and L.T. Wheeler, "The application of a homogeneous half-space model in the analysis of endothelial cell micropipette measurements," *Trans. of the ASME*, Vol. 110, pp. 190-199, 1988.

[8] M. Sato, D.P. Theret, L.T. Wheeler, N. Ohshima, and R.M. Nerem, "Application of the micropipette technique to the measurement of cultured porcine aortic endothelial cell viscoelastic properties," *J. of Biomech. Eng.*, Vol. 112, pp. 263-268, 1990.

[9] E. Evans, and A. Yeung, "Apparent viscosity and cortical tension of blood granulocytes determined by micropipette aspiration," *Biophys. J.*, Vol. 56, pp. 151-160, 1989.

[10] D. Needham, and R.M. Hochmuth, "Rapid flow of passive neutrophils into a 4μm pipet and measurement of cytoplasmic viscosity," *J. of Biomech. Eng.*, Vol. 112, pp. 269-276, 1990.

[11] D.E. Discher, D.H. Boal, and S.K. Boey, "Simulations of the erythrocyte cytoskeleton at large deformation II: Micropipette aspiration," *Biophys. J.*, Vol. 75, pp. 1584-1597, 1998.

[12] W.R. Jones, H.P.T. Beall, G.M. Lee, S.S. Kelley, R.M. Hochmuth, and F. Guilak, "Alterations in the Young's modulus and volumetric properties of chondrocytes isolated from normal and osteoarthritic human cartilage," *J. of Biomech.*, vol. 32, pp. 119-127, 1999.

[13] N. Otsu, "A threshold selection method from gray-level histograms," *IEEE Trans. Systems Man. Cybernet.*, Vol. 9, No. 1, pp. 62—66, 1979.

[14] W. Zhi, Q. Li, S. Zhong, and S. He, "Fast adaptive threshold for the Canny edge detector," Prof of SPIE, Vol. 6044, 60441Q, 2005.

[15] X.Y. Liu, W.H. Wang, Bob M. Lansdorp, and Y. Sun, "Cellular force measurement using an elastic microfabricated device," IEEE/RSJ Int. Conf. Intell. Robots Sys., Beijing, 2006.

[16] S.P. Maybeck, *Stochastic Models, Estimation, and Control,* Vol. 1, 1979, Academic Press, Inc.

[17] W.D. Merryman, I. Youn, H.D. Lukoff, P.M. Krueger, F. Guilak, R.A. Hopkins, and M.S. Sacks, "Correlation between heart valve interstitial cell stiffness and transvalvular pressure: implications for collagen biosynthesis," *Am. J. Physiol. Heart Circ. Physiol.*, Vol. 290, No. 1, pp. 224-231, 2005.